Heliyon 10 (2024) e39450

Contents lists available at ScienceDirect

Heliyon

journal homepage: www.cell.com/heliyon

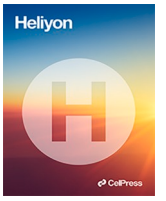

Research article

Synthesis and characterization of nano iron oxide biochar composite for efficient removal of crystal violet from water

T. Geetha [a,*], John K. Smitha [b], Manju Sebastian [c], Mathew Irimpan Litty [c], Bincy Joseph [c], Jincy Joseph [c], T.S. Nisha [c]

[a] Dept. of Chemistry, Vimala College (Autonomous), Thrissur, Kerala, 680009, India
[b] Dept. of Soil Science and Agricultural Chemistry, Kerala Agriculture University, Thrissur, Kerala, 680656, India
[c] Dept. of Chemistry, St. Mary's College, Thrissur, Kerala, 680020, India

ARTICLE INFO

Keywords:
Coconut husk
Biochar
Magnetic
Nano iron oxide
Crystal violet
Adsorption

ABSTRACT

In the present study, Coconut Husk Biochar (CHB) was synthesize from widely available, locally sourced agro waste, coconut husk and characterized using different techniques like scanning electron microscopy (SEM), Brunauer-Emmett-Teller (BET) analysis, Fourier-transform infrared spectroscopy (FTIR) and X-ray diffraction (XRD). CHB was tested for its ability to adsorb crystal violet (CV), a commonly used cationic dye, from water. It was capable of adsorbing more than 98 % of CV from water and follows Freundlich isotherm model with pseudo second order kinetics though the overall process was unfavourable. Moreover, separation of CHB from water after adsorption is a cumbersome process. Thus, unmodified CHB is not suitable for use as an adsorbent for CV. Magnetic nano iron oxide Biochar Composite (MBC) was synthesized by deposition of nano iron oxide (Fe_3O_4) onto its surface by co-precipitation method and characterized using SEM, XRD and FTIR. SEM analysis provided visual evidence of this deposition which was further confirmed by XRD and FTIR analysis. MBC was also effective in adsorbing more than 90 % of CV from aqueous solution though a decrease in adsorption capacity was observed. Adsorption data followed Langmuir isotherm model and pseudo second order kinetics. MBC is superparamagnetic and is strongly attracted to a small bar magnet, facilitating easy removal from water after CV adsorption.

1. Introduction

Water is connected with every form of life on earth and clean drinking water is essential to all living beings. Unfortunately, sources of clean drinking water are becoming scarce as they are contaminated by physical and chemical contaminants. In countries with rapidly developing industrial sectors, contamination by untreated or inadequately treated industrial effluent is a growing concern. Large scale pollution caused by industrial effluents has been documented in major river such as Ganga [1] and Narmada in India [2], Ravi in Pakistan [3], Buriganga and Karnaphuli river in Bangladesh [4,5] and Min River in China [6].

Industries as varied as textiles, leather, paints, photography, cosmetics, pharmaceutical products and food, use dyes to impart colour. Dyeing requires copious amounts of water, and the resulting discharge often has a significant dye content ranging from 1 to 15 % [7,8]. If untreated, the dye-contaminated water eventually finds its way into natural water bodies and can remain in the

* Corresponding author.
E-mail address: drtgeetha@vimalacollege.edu.in (T. Geetha).

https://doi.org/10.1016/j.heliyon.2024.e39450
Received 7 May 2024; Received in revised form 14 October 2024; Accepted 15 October 2024
Available online 17 October 2024

environment for an extended period of time. The presence of dye in water, even in small quantities, seriously affects the transparency and quality of water bodies such as lakes and rivers. The reduced passage of sunlight leads to lowered photosynthetic activity and oxygen concentration in the water thus damaging the aquatic environment. The toxicity, mutagenicity, and carcinogenicity of many of these dyes and their degradation products are also inimical to aquatic life [9–11].

Crystal violet (CV) ($C_{25}H_{30}N_3Cl$), a triarylmethane dye, is one of the most abundantly used cationic dyes in the textiles, paint, medical and biotechnology industries worldwide. Due to its complex aromatic structure and synthetic origin, CV, a highly toxic dye, is poorly metabolized by microbial flora and persists in the environment for long periods [12–14]. Cationic dyes are also more toxic than anionic dyes as they interact easily with the negatively charged cell membrane [15]. It is a well-known mutagen, teratogen, carcinogen and causes mitotic poisoning [16]. Therefore, it is essential to remove CV from water utilizing efficient environmentally friendly, cost-effective technologies.

Various processes are used to remove dyes from aqueous solutions. These include filtration [17], ultrafiltration [18], photocatalytic degradation [19], electrochemical treatments [20], ozonation [21], electrocoagulation/flotation [22], reverse osmosis [23], microbial degradation [24] and adsorption [25]. Although these techniques are capable of removing dyes from water, adsorption is the most preferred method due to its simplicity, efficiency, affordability, minimal maintenance and absence of toxic by-products [26–30]. An adsorbent that is abundantly available, inexpensive and non-hazardous will considerably lower the cost of treatment of contaminated water [31]. Biochar, a carbon-rich material produced from organic feedstock under limited oxygen by thermal decomposition has recently gained considerable interest as it satisfies the above-mentioned criteria. This is especially true in the case of biochar prepared from inexpensive feedstock's like agricultural waste as they are cost-effective, and economical [32,33].

Coconuts, a commercially important crop that yields oil, food, animal feed, and fiber, is widely found in Southeast Asia, the Pacific region, Latin America and Africa. The inedible, fibrous, rough outer shell of coconut fruit, coconut husk, is an agricultural waste that is voluminous and difficult to manage. Of the 8,000,000 tons produced annually, a small fraction is converted into commercially valuable products like coir fibre, furnishing, decorative articles, potting mixture etc. and the rest is discarded or burnt causing environmental problems [34–40]. Conversion of coconut husk, which is a cheap, widely available agricultural waste material, into biochar, and its use as an adsorbent for dyes from wastewater is thus economically feasible and environmentally sound.

The more widespread and large-scale application of biochar is limited by its small particle sizes and low density, which makes it difficult to separate and reuse it. Release of biochar into natural waters may cause secondary pollution by enhancing the migration and resuspension of pollutants in the sediments. This problem can be solved by magnetizing biochar as it can then be removed easily and rapidly from aqueous media by magnetic separation. This streamlines the separation process, lowers energy consumption and increases reusability [40–43].

Biochar has been produced from organic matter generated during the cultivation, processing, and consumption of coconuts. Various parts of coconut tree like leaves, husks, fronds, and shells, have been converted into biochar and used for soil remediation and remediation of heavy metals, phenols and antibiotics contaminated water [44–47]. However, no attempt has yet been made to produce coconut husk biochar, magnetize it and use it for treatment of dye contaminated water. To the best of our knowledge, this study is the first to report the conversion of coconut husk to biochar and modified magnetic biochar capable of adsorbing crystal violet from water. The significance and relevance of the study lies in the fact that it converts a difficult to dispose of agri-waste, coconut husk, to an adsorbent that may aid environmental remediation by treating dye contaminated industrial effluents.

The objective of the study was to synthesize Coconut Husk Biochar (CHB) from locally sourced coconut husk by heap method and to characterize it using various spectroscopic and microscopic techniques. To simplify the removal of biochar following the adsorption process, we magnetized CHB by depositing iron oxide nanoparticles on it using the co-precipitation method. The synthesized Magnetic nano iron oxide Biochar Composite (MBC) was also characterized using above mentioned techniques. Adsorption studies of CHB and MBC were carried out to determine optimum dose and contact time of biochar and to identify the best fitting isotherm. The attraction of MBC to a simple bar magnet was tested and its magnetic property measured using VSM.

2. Materials and methods

2.1. Materials

All the chemicals and reagents used are of AR grade and used without further purification. Crystal Violet ($C_{25}N_3H_{30}Cl$), Sodium chloride (NaCl), Sodium hydroxide (NaOH), Mohr's salt ($Fe(SO_4)\ (NH_4)_2(SO_4).6H_2O$) and Ferric Chloride ($FeCl_3.6H_2O$) were purchased from Merck, India. Coconut husk was sourced locally from Kerala Agricultural University, Thrissur, India.

2.1.1. Preparation of coconut husk biochar

CHB was prepared by heap method [48]. The coconut husk was sourced locally, washed repeatedly with water to remove dirt and foreign objects and then dried in the sun. The husk was then cut into small pieces. These pieces were heaped inside a kiln specially fabricated for biochar production. The material inside the kiln was lit and the fire spread around to allow anaerobic burning before closing the lid. Smoke was allowed to escape through the vents. After the smoke escaped, the vents were closed, and the sides of the lid plastered using mud. The temperature of pyrolysis was 340 °C with a residence time of 24 h. Biochar was collected the very next day.

2.1.2. Synthesis of magnetic nano iron oxide biochar composite

Magnetic nano iron oxide Biochar Composite (MBC) was synthesized by co-precipitation method [41]. In an Erlenmeyer flask, 50 mL of Mohr's salt solution (0.1M) and 100 mL of Ferric chloride solution (0.1M) were taken and stirred for 1 h on a magnetic stirrer.

Five grams of biochar was added to these and the stirring continued for another 30 min pH of the solution was raised to 11.5 by the addition of 0.1M NaOH solution. The solution was stirred continuously for another 2 h, filtered and washed repeatedly to obtain MBC.

2.2. Characterization of biochar

The bulk density and pH of CHB and MBC were determined. The bulk density was determined using equation (1) below

$$\text{Bulk density} = \frac{\text{Mass of the dry sample(g)}}{\text{Volume of dry sample } (\text{cm}^3)} \quad (1)$$

The pH was determined after 1 gm of sample was agitated with 20 ml of double distilled water for approximately 5 min on a magnetic stirrer. The BET surface area (S_{BET}), pore size and pore volume of biochar samples was determined by N_2 adsorption at 77 K on BELSORP-max, an automatic gas adsorption measuring unit. Prior to analysis, the samples were degassed under continuous nitrogen flow for 12 h at 150 °C. Scanning electron microscopy (SEM) was used to visualize the microstructure of CHB and MBC. The surface morphology was observed using Gemini SEM 300 Field Emission Scanning Electron Microscope. The functional group on the surface of biochar samples was determined using Fourier Transform Infrared spectroscopy (FTIR; Agilent Cary 620 FTIR Imaging system). The FTIR spectra were recorded in wavelengths ranging from 400 to 4000 cm^{-1}. The X-ray diffraction (XRD) pattern was collected on an X-ray diffraction system (PANALYTICAL, Aeris Research) with Copper Kα radiation (λ = 1.54060 Å) over the 2θ range 5°–90°, operating at 36 kV and 36 mA using a step size of 0.04° and a scan speed of 36 s/step. The presence or absence of magnetic property was identified by its behaviour towards the bar magnet and if magnetic property was demonstrated by the sample, it was measured using a vibrating sample magnetometer (VSM).

2.3. Adsorption studies

2.3.1. Determining best concentration of dye solution and optimal dose of biochar

In order to establish the ideal concentration of CV for adsorption studies, we prepared CV solutions at concentrations of 50, 100, 200, and 300 mg/L. Subsequently, 0.6 g of biochar was added to each 100 mL of the dye solution, shaken on a rotary shaker at room temperature for 24 h, centrifuged for 10 min at 4000 rpm, filtered and the concentration determined using a double beam UV–Visible Spectrophotometer (Shimadzu). The adsorption percentage of the dye was calculated using equation (1) below and the solution with highest value used for determining optimum dose of biochar.

To determine optimum dosage of biochar, batch adsorption experiments were conducted. Different doses of biochar viz, 0.2, 0.4, 0.6, 0.8, 1.0, 1.2, 1.4, 1.6 and 2.0 g, were added to 100 mL of CV dye solution and shaken on a rotary shaker at room temperature for 24 h. The solution was then centrifuged for 10 min at 4000 rpm, filtered and the concentration determined using a double beam UV–Visible Spectrophotometer (Shimadzu). Adsorption experiments were conducted in duplicate and the average values are reported here. The adsorption percentage of the dye and adsorption capacity of the adsorbent material, Q_t (mg/g), was calculated using equations (2) and (3) below

$$\text{adsorption percentage} = \frac{(C_0 - C_t) \times 100}{C_0} \quad (2)$$

$$\text{adsorption capacity } (Q_t) = \frac{(C_0 - C_t) \times V}{W} \quad (3)$$

where C_0 and C_t are the concentration of the dye in mg/L at the start of the experiment and at the time of sampling. V is the volume (in L) of dye solution and W is the weight of the biochar.

2.3.2. Adsorption kinetics

The absorption of CV on CHB and MBC was investigated as a function of contact time at room temperature. Adsorbent dosage and initial dye concentration were maintained at their optimum value for this experiment. The optimum dose of each biochar was weighed into ten conical flasks, each containing 100 mL of crystal violet solution and then agitated on a rotary shaker for 3 h. At 5, 10, 15, 30, 45, 60, 90, 120, 150 and 180 min respectively, the solution was centrifuged, filtered and the concentration of filtrate determined. The data obtained were evaluated for their fit of pseudo-first order (equation (4)) and pseudo-second order (equation (5)) models to understand adsorption processes, underlying mechanisms and possible rate controlling steps [49–52].

The Pseudo-first-order Kinetic Equation (Linear form)

$$\ln(q_e - q_t) = ln\, q_e - k_1 t \quad (4)$$

The Pseudo-second-order Kinetic Equation (Linear form)

$$\frac{t}{q_t} = \frac{t}{q_e} + \frac{1}{k_2\, q_e^2} \quad (5)$$

where q_t (mg/g) is amount adsorbed at time t, q_e(mg/g) is the amount adsorbed at equilibrium, k_1 is the pseudo-first-order rate constant (L/min) and k_2 is the pseudo-second-order rate constant (g/mg.min)

2.3.3. Adsorption isotherm

The adsorption isotherm models described the relationship between the amount of adsorbate adsorbed on the adsorbent (Q_e) and liquid phase concentration of adsorbate (C_e) at equilibrium conditions at a constant temperature [53]. For adsorption of dyes on to biochar, the two parameter isotherm models namely Freundlich, Langmuir, Temkin, Harkins Jura, Elovich and Dubinin Raduskevich are commonly used to explain this relationship. The Langmuir isotherm model, an empirical model, assumes that the adsorption surface is homogeneous and exhibits equal affinity toward the adsorbate. In this model, it is postulated that adsorbate molecules compete to bind with the active sites, which are specific and localized, forming a monolayer on the adsorbent's surface with minimal lateral interaction among them.

On the other hand, the Freundlich isotherm model, Harkins Jura Isotherm model, Elovich isotherm model and Dubinin Raduskevic isotherm model, all permit multilayer adsorption. In Freundlich isotherm model the surface of adsorbate is considered heterogeneous in nature with varying affinity toward the adsorbent. The Harkins Jura Isotherm model takes into account the existence of pores of various sizes on the surface of biochar while Temkin isotherm considers both adsorbent-adsorbate interactions and the fact that the heat of adsorption decreases linearly with coverage. Elovich isotherm, based on kinetic principles, postulates that adsorption sites increase exponentially with adsorption while Dubinin Raduskevic isotherm proposes that adsorption involves pore filling, with Gaussian energy distribution. In this study we used the linearized form of the isotherms which were fitted to adsorption data and their suitability determined by comparing coefficient of regression. The Adsorption isotherms, linearized equations and their plots used in the study are given in Table 1 [54–58].

Where C_e (mg/L) represents concentration of dye at equilibrium, Q_e (mg/g) and Q_m (mg/g) are adsorption capacity of dye at equilibrium and saturation, respectively, K_L(L/mg) is the Langmuir constant, K_F (mg/g) is the Freundlich constant, and 1/n is the adsorption intensity factor or surface heterogeneity. A and B are the Harkins Jura isotherm constant. A_T is the equilibrium binding energy or the optimum binding energy (L/g), R the universal gas constant and B_T, the Temkin constant at temperature T (in Kelvin) where (J/mol) is a constant related to the heat of adsorption. Q_0 is the maximum adsorption capacity (mg g^{-1}), and K_E is the equilibrium constant of Elovich isotherm (L mg^{-1}). Q_s is the theoretical isotherm saturation capacity (mg/g) and ε is the Dubinin–Radushkevich isotherm constant. The analysis was conducted by placing 100 mL of CV dye solution in 250 mL flasks with different adsorbent dosages (0.02–2 g). The adsorption capacity and equilibrium solution concentrations were then measured and the suitability of the isotherm investigated.

3. Results and discussions

3.1. Biochar characterization

3.1.1. Bulk density, pH and PZC

The bulk density of a biochar determines its floatability and sinkability, a crucial factor in designing commercial adsorption columns. The lower limit on bulk density set by the American Water Work Association is 0.25 g/cm^3 [59]. The values for both CHB and MBC were found to be higher than recommended (0.3204 g/$cm^3$for CHB and 0.5946 g/cm^3 for MBC) indicating its suitability as an absorbent in wastewater treatment. The higher bulk density value of MBC compared to CHB can be attributed to the iron oxide (Bulk density 5 g/cm^3) that has been impregnated in biochar. The pH values of CHB and MBC were found to be 9.3 and 5.97, respectively. The PZC of the adsorbents gives us an insight into the charge on the surface of the adsorbent at a particular pH. When the pH of the medium equals that of the PZC, the surface of the adsorbent does not carry any charge [60]. The point of zero charge (PZC) was determined to be 8.9 for CHB and 8.5 for MBC. A similar decrease in PZC on magnetization has been previously reported by Trinh et al., [61]. In the case of CHB, the pH value exceeded the PZC, resulting in a negatively charged surface that facilitates the attraction of cationic dyes such as crystal violet. Conversely, the pH of MBC was below the PZC, leading to a positively charged surface that may induce electrostatic repulsion, thereby decreasing its adsorption capacity for crystal violet.

Table 1
Adsorption isotherm, its linearized form, parameters and plot for graphical representation.

Isotherm	Equation	Linearized equation	Plot
Freundlich	$Q_e = K_F C_e^{1/n}$	$ln\ Q_e = ln\ K_F + \frac{1}{n} ln\ C_e$	$ln\ Q_e$ vs $ln\ C_e$
Langmuir	$Q_e = \frac{Q_m K_L C_e}{1 + K_L C_e}$	$\frac{1}{Q_e} = \left(\frac{1}{Q_m K_L}\right)\frac{1}{C_e} + \frac{1}{Q_m}$	$\frac{1}{Q_e}$ vs $\frac{1}{C_e}$
Harkins Jura	$Q_e = \left(\frac{A}{B - log\ C_e}\right)^{1/2}$	$\frac{1}{Q_e^2} = \frac{B}{A} - \left(\frac{1}{A}\right) log\ C_e$	$\frac{1}{Q_e^2}$ vs $log\ C_e$
Temkin	$Q_e = \frac{RT}{b_T} \ln (A_T C_e)$	$Q_e = \frac{RT}{b_T} ln\ A_T + \frac{RT}{b_T} ln\ C_e$	Q_e vs $ln\ C_e$
Elovich	$\frac{Q_e}{Q_0} = K_E C_e e^{-\left(\frac{Q_e}{Q_0}\right)}$	$ln\left(\frac{Q_e}{C_e}\right) = ln\ K_E Q_0 - \frac{Q_e}{Q_0}$	$ln\left(\frac{Q_e}{C_e}\right)$ vs Q_e
Dubinin Raduskevic	$Q_e = Q_s e^{-K\varepsilon^2}$	$ln\ Q_e = Q_s - k\varepsilon^2$	$ln\ Q_e$ vs ε^2

3.1.2. Specific surface area and porosity

Specific surface area and porosity are two important physical properties that influence the adsorption capacity of biochars. The specific surface area of CHB obtained by N_2 adsorption–desorption isotherm is 25.24 m^2g^{-1}. This value is comparable to the specific surface area of biochar obtained from agricultural by-products like corn straw (15.12 m^2g^{-1}) and maize straw (70 m^2 g^{-1}) [62,63], higher than the specific surface area of biochar obtained from Eucalyptus sawdust (1.57 m^2g^{-1}) and durian wood (2.5 m^2g^{-1}) [64,65] and lower than the specific surface area of biochar obtained from Coconut shell (279 m^2g^{-1}), and from pulp and paper sludge (174.29 m^2/g) [66,67]. Upon magnetization the value increased exponentially to 1162.75 m^2g^{-1}. This dramatic increase in surface area may be attributed to the deposition of nano iron oxide onto the surface of biochar (Fig (a and b)). A similar increase of surface area on deposition of nanoparticles onto biochar matrix has been previously reported in literature [43,68].

Occurrences and diversity of pores in biomass is due to the loss of water and releases of volatile constituents from the carbon matrix during pyrolysis. The size of pores often ranges from nanometers to micrometers in scale and can be divided into three groups: micropores (<2 nm), mesopores (2–50 nm), and macropores (>50 nm) [69,70]. From BET and BJH data it can be concluded that pores in both biochar are a mixture of meso and macropores spanning the nano-region (1–100 nm). The BJH plot of CHB and MBC are shown in Fig. 1(b and c). The average pore diameter and total pore volume was quantified to be 20.47 nm and 0.023372 cm^3g^{-1} for CHB. For MBC the average pore diameter was found to be significantly lower (2.26 nm) but total pore volume was higher (0.08234 cm^3 g^{-1}). This may be credited to the presence of micropores in MBC which was not observed in CHB. The reduced average pore diameter of MBC may account for its lower adsorption capacity, despite its higher specific surface area and pore volume, as the average pore diameter (2.26 nm) closely approximates the molecular size of crystal violet (1.4 × 1.4 nm).

3.1.3. SEM analysis

The SEM images of the prepared CHB and MBC samples at different magnifications are shown in Fig. 2. It is clear from the SEM image (a) that the particles of CHB are small though heterogeneous in size (2–32 μm). Particles are of an irregular shape with uneven edges and a rough and porous surface.

A closer look at biochar surface shows micro, meso and macropores on the surface of biochar (image b). SEM image (c) shows that the surface of MBC is covered with nano iron oxide. The nano iron oxide particles are observed to be deposited in an irregular manner.

3.1.4. Fourier Transform Infrared spectroscopy (FTIR)Analysis

FTIR spectroscopy was used to identify various functional groups on the surface of the biochar and to confirm the formation of iron oxide. For both CHB and MBC, a strong broad band at around 3400 cm^{-1} (Fig. 3.) may be assigned to stretching vibration of the hydroxyl group (-OH) probably originating from the moisture content of the biochar or from alcoholic or phenolic (-OH) groups on the surface of biochar. Both the biochar shows a doublet at 2339 and 2360 cm^{-1} corresponding to presence of CO_2 in the micropores at a concentration higher than atmospheric concentration [71,72]. A broad peak at 2000 cm^{-1} could be due to the C-H or C=C stretch of the aromatic rings [73]. The weak band at 1752 cm^{-1} is due to the in-phase aromatic C=C stretching vibrations [74] and the band at 1718 cm^{-1} due to C=O stretching peak of carbonyl group [75]. The peak at 1575 cm^{-1} and the one at 1382 cm^{-1} are due to the asymmetric and symmetric C-O vibration band of carboxylic acid group on the surface of biochar [76]. The strong broad peak at

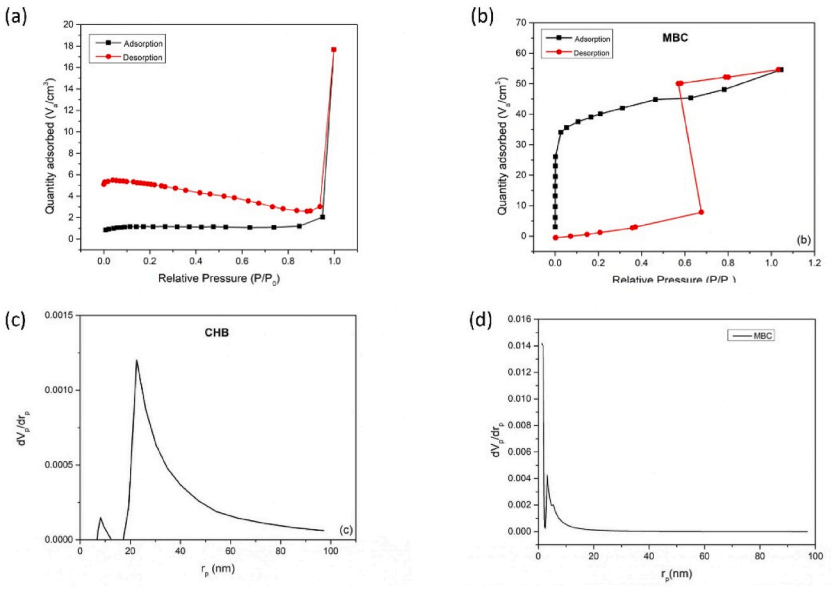

Fig. 1. BET nitrogen adsorption-desorption isotherm of (a) Coconut husk biochar and (b) Magnetic nano iron oxide biochar composite; BJH pore size distribution curve of (c) Coconut husk biochar and (d) Magnetic nano iron oxide biochar composite.

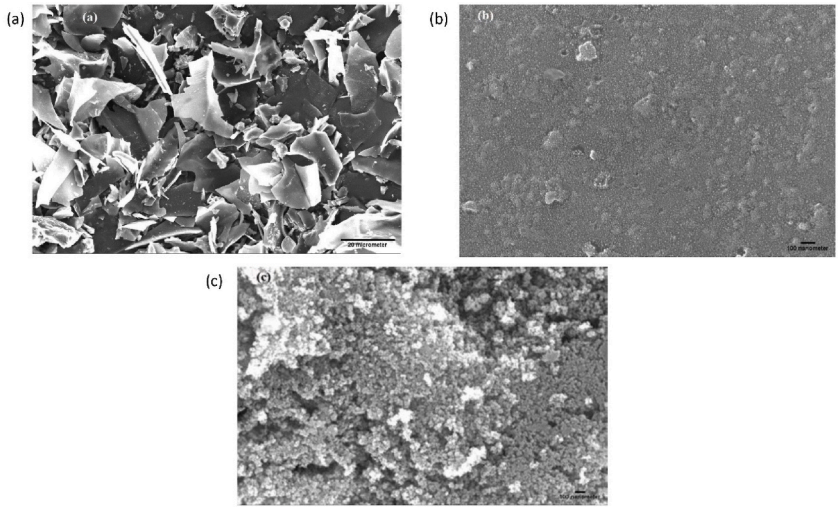

Fig. 2. (a and b) SEM image of Coconut husk biochar and (c) Magnetic nano iron oxide biochar composite.

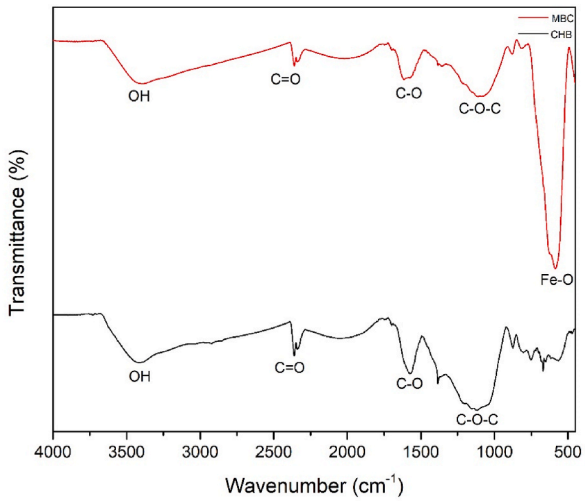

Fig. 3. Fourier Transform Infrared spectra of Coconut Husk Biochar and Magnetic nano iron oxide Biochar Composite.

around 1100 cm^{-1} may be due to C-O-C symmetrical stretching, characteristic of cellulose and hemicellulose. The multiple peaks observed in the region between 700 and 900 cm^{-1} may be assigned to out of plane vibration of aromatic C-H bonds [77,78].

In the case of magnetic biochar, the emergence of an additional strong peak at 584 cm^{-1} was observed. This peak corresponds to the Fe–O bond of iron oxide (Fe_3O_4) suggesting the formation and loading of iron oxide onto biochar [79,80]. Spectral analysis of CHB suggests the presence of oxygen containing groups like -COOH and -OH on the surface. It is possible that iron oxide may be anchored to the surface of biochar by binding with these groups through electrostatic interactions or by covalent bonding [81].

3.1.5. X-ray diffraction (XRD) analysis

The XRD pattern of CHB (Fig. 4) is characterised by diffuse, broad bands indicative of short-range order in biochar, while the sharp and narrow peaks are due to highly crystalline phases with high degree of long-range order [80]. The broad peak centered at around 2θ value is 23.5 and indexed as C (002) diffraction peak indicating amorphous carbon structure with randomly oriented aromatic sheets. Sharp peaks were observed at 2θ values 28.3, 40.5, 50.2, 66.3 and 73.6 respectively and can be assigned to KCl (Sylvite). This may correspond to the ash and tarry material trapped within the pores of the biochar sample [82,83].

The Powder X Ray Diffraction pattern of MBC was performed to confirm the loading of nano iron oxide onto biochar. The XRD pattern of MBC (Fig. 5) shows five peaks at 2θ values of 30.3496, 35.7027 (100 % intensity), 43.3332, 57.2826 and 62.9045.

The pattern matches that of iron oxide particles corresponding to Fe_3O_4 (Reference no. 01-075-1609) thus confirming the synthesis and loading of iron oxide onto biochar. To determine the crystallite size of loaded nano iron oxide, peak broadening of the most intense peak was used and the average size of the Fe_3O_4 particle was found to be 28 nm. This confirms that the MBC synthesized is a

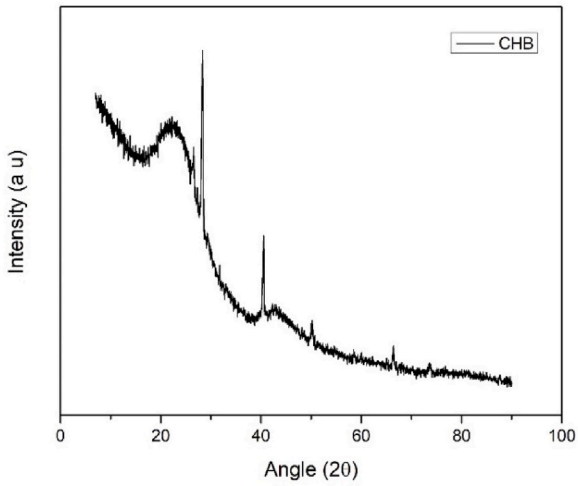

Fig. 4. X ray Diffraction pattern of Coconut Husk Biochar.

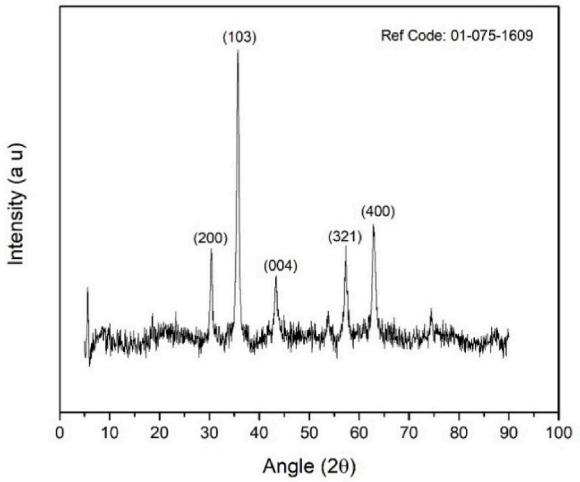

Fig. 5. X ray Diffraction pattern of Magnetic nano iron oxide Biochar Composite.

nanocomposite.

3.1.6. Vibrating sample magnetometer (VSM) analysis

The magnetic behaviour of the prepared MBC was verified using an external magnet. The particles are strongly attracted to the external bar magnet. In an aqueous environment, this strong magnetic response facilitates the separation of MBC particles after adsorption as they rapidly accumulate under the influence of magnetic field, as illustrated in Fig. 6(a) [84]. The magnetic property of the material is investigated further using vibrating sample magnetometer (VSM) analysis and the magnetization curve is shown in Fig. 6(b). The curve indicates that the MBC demonstrates superparamagnetic behaviour characterized by the absence of a hysteresis loop [85] with a saturation magnetization value is 26.4 emu/gm.

4. Adsorption studies

4.1. Adsorption studies of CHB and MBC

A preliminary study was conducted to determine the optimal concentration of the dye for adsorption studies. The optimal CV concentration was determined to be 200 mg/L for CHB and 100 mg/L for MBC, respectively. CHB was capable of adsorbing 98 % of CV from water. The percentage of CV removed was directly proportional to the quantity of adsorbent used, as an increased adsorbent quantity offers a greater surface area, thereby enhancing dye adsorption. This trend persisted until an optimum value beyond which there was no concomitant increase in dye removal. Moreover, a small decrease in the ability of biochar to remove dye was also noticed.

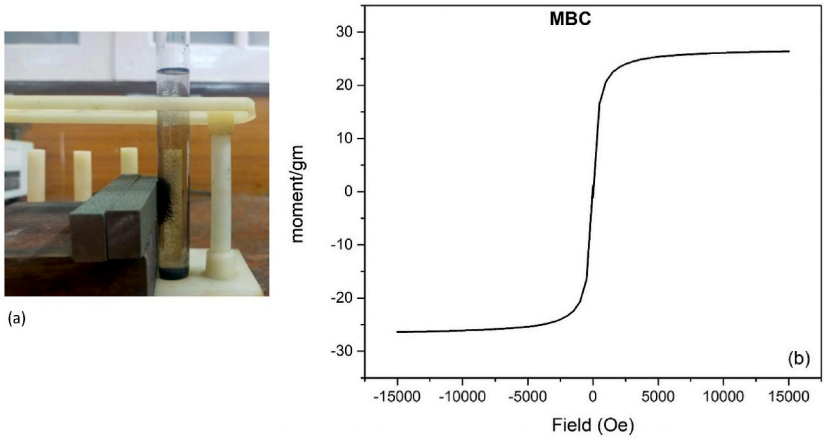

Fig. 6. (a) Magnetic separation of Magnetic nano iron oxide biochar composite in aqueous environment using a simple bar magnet and (b) its VSM image.

This decrease may be attributed to the aggregation of the adsorbent at high concentration and consequent decrease in surface area [86]. A linear relationship between percentage of CV removed and quantity of absorbent was also true in the case of MBC. It was capable of removing 90 % of the dye from water. The optimum dose of biochar was determined to be 0.7 g/L for CHB and 2.0 g/L for MBC (Fig. 7).

The interaction between adsorbent and adsorbate may involve ionic interactions, electron donor acceptor interactions, hydrogen bonds, π-π attractions and van der Waals interactions. Presence of oxygen containing functional groups like -OH, Fe-O, -COOH on the surface of biochar may facilitate hydrogen bonds and π-π attractions with CV. Further discussion on the mechanism of adsorption of CV onto CHB and MBC is given in greater details later in the manuscript.

4.2. Adsorption kinetics

The adsorption of crystal violet (CV) onto biochar increased over time. For CHB, the equilibrium was quickly attained within 10 min of contact, whereas the equilibrium time for the magnetized biochar composite (MBC) was observed to be 3 h. In both cases, the initial adsorption of CV was rapid, followed by slower rate of adsorption and a subsequent equilibrium stage. The initial rapid adsorption could be attributed to the availability of large number of adsorption sites for CV. Over time, the adsorption sites become occupied and the rate of adsorption progressively decreases, eventually reaching equilibrium [87].

The pseudo-first order and pseudo-second-order kinetic model equations were applied on the adsorption data obtained from the experiments (Fig. 8). In both instances, the data was more suitable for pseudo second order kinetic model than pseudo first order kinetic model. The experimental q_e value was found to be closely aligned to the calculated q_e value derived from the pseudo-second order kinetic model further supporting its suitability to the system (Table 2).

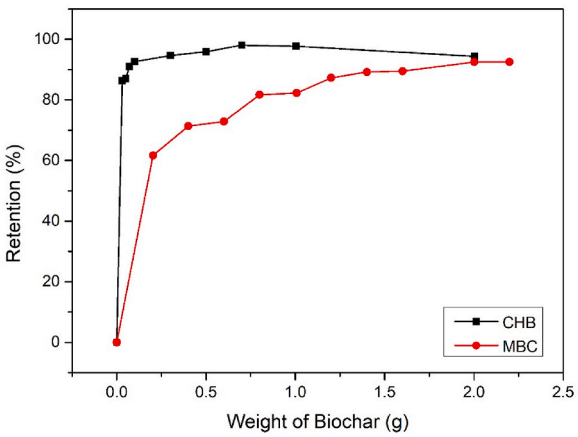

Fig. 7. Effect of adsorbent dosage on the retention percentage of crystal violet at 25 °C with a contact time of 180 min on Coconut husk biochar (initial crystal violet concentration of 200 mg/L) and Magnetic nano iron oxide biochar composite (initial crystal violet concentration of 100 mg/L). (For interpretation of the references to colour in this figure legend, the reader is referred to the Web version of this article.)

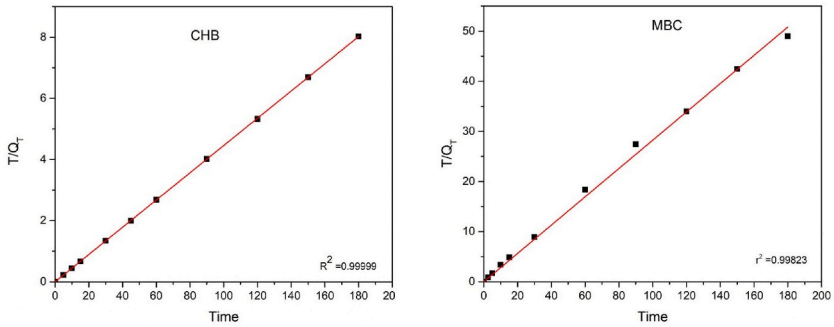

Fig. 8. Kinetics modelling using pseudo-second order models for Coconut Husk Biochar and Magnetic nano iron oxide Biochar Composite.

The observed maximum adsorption capacity of CHB, 25.5 mg/g, compares well with previously reported materials for crystal violet adsorption listed in Table 3. This comparison indicates that the adsorption capacity of CHB is higher than that of biochar prepared from sugarcane and Gliricidia sepium wood and comparable to that of biochar prepared from sugarcane filter mud, date palm petioles, chinnar leaf and palm kernel shell. However, on magnetization by impregnating with iron oxide, there is a noticeable decrease in adsorption capacity.

4.3. Adsorption isotherm

Crystal violet adsorption by CHB follows the Freundlich isotherm model better than Langmuir, Harkins Jura, Elovich, Temkin and Dubinin Raduskevic model as its coefficient of determination was the highest (Table 4 and Fig. 9). Freundlich isotherm model describes a reversible multilayer adsorption on to a heterogeneous substance with non-uniform distribution of affinity across the surface of biochar. As the surface of biochar is heterogeneous in nature and encompasses pores of various sizes including meso and macropores, it is understandable that Freundlich isotherm model provided the most accurate fit. The presence of various functional groups on the surface of biochar may account for the presence of adsorption sites of varying affinities and strength [88,89]. The 1/n value of the Freundlich isotherm was greater than 1(1.5969) which suggests that the adsorption process is unfavourable and the bonds between adsorbate and adsorbent are weak. Thus, the use of CHB to adsorb dye from wastewater may not be feasible without further modification as the adsorbed crystal violet may easily be desorbed back. Moreover, the separation of biochar from aqueous medium after the completion of adsorption is both difficult and time consuming.

To address both challenges simultaneously, we modified CHB by depositing nano iron oxide particle on to its surface. The data from adsorption studies on MBC was found to be more suited to the Langmuir isotherm model than that of Freundlich, Harkins Jura, Temkin, Elovich and Dubinin Raduskevic models (Table 3 and Fig. 9).

The stability constant of the Langmuir model was 0.000029, indicating that the adsorption process was highly favourable ($0 < R_L < 1$). The Langmuir model assumes that all the sites for adsorption are homogeneous, possess equal energy, and support the formation of a monolayer on the adsorbent surface. In contrast, the Freundlich isotherm model allows for multilayer adsorption. The dense deposition of nano iron oxide on the biochar surface may have significantly altered its structure, making the adsorption process highly favourable. This shift from a multilayer to a monolayer adsorption model also accounts for the reduced Q_{max} value of MBC compared to CHB [98,99].

4.4. Adsorption mechanism

The interaction between biochar and cationic dyes like crystal violet may include both physisorption and chemisorption. The Vander-Waals forces of attraction, hydrogen bonds, π–π electron donor acceptor interactions, all contribute to the physisorption of CV. Chemisorption, on the other hand predominantly utilizes the electrostatic interactions between the negatively charged biochar surface and positively charged CV molecule. The FTIR spectra of CHB indicate the presence of various functional groups, such as hydroxyl groups, carbonyl groups, carboxylic groups, and aromatic rings, on the surface of the biochar. The amine group of CV may form hydrogen bond with hydroxyl and carboxylic acid group on biochar surface. The role of surface functional groups like hydroxyl groups in regulating the absorption of contaminants have been reported in previous studies [100]. The protonated amine group of CV may also be electrostatically attracted towards either the carboxylate anion or the phenoxide anion on biochar surface. The size of CV (1.4 nm × 1.4 nm) allows it to easily enter into pores and interact with the inner surface are. The adsorption of crystal violet on biochar may also be facilitated by π–π interactions between aromatic ring on the biochar surface and the benzene ring of crystal violet (Fig. 10) [91, 101–103].

Electrostatic attraction between iron oxide loaded on biochar and chloride ion of CV may aid in adsorption of the dye on to MBC. Interactions between iron oxide loaded biochar and cationic dyes have also been reported in previous studies, supporting the suggested mechanism [97,104].The deposition of Fe_2O_3 onto biochar led to a rapid increase in the surface area of MBC compared to CHB. This increase in surface area was accompanied by a significant decrease in pore size probably due to the deposition of iron oxide on the rims.

Table 2
Comparison of correlation coefficient, Exp.Q_e, Cal. Q_e and equilibrium time of CHB and MBC.

	R^2	Exp. Q_{max}. (mg/g)	Cal. Q_{max}. (mg/g)	Equilibrium Time
CHB	0.9999	25.15	22.42	10 mints
MBC	0.9975	3.67	3.63	3 h

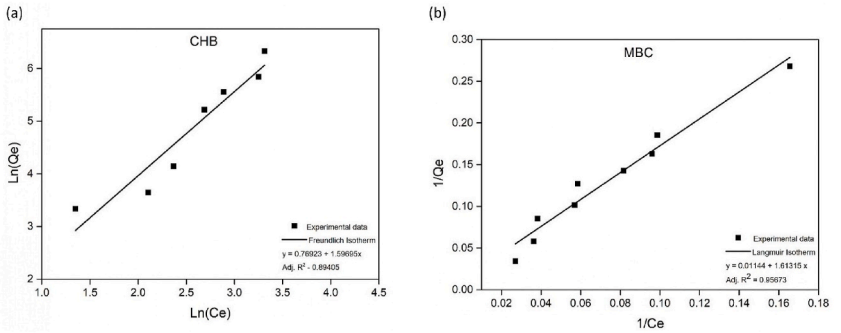

Fig. 9. The linear fitting of (a) Freundlich adsorption isotherm of Coconut husk biochar (b) Langmuir adsorption isotherm of Magnetic nano iron oxide biochar composite.

Table 3
Comparison of maximum adsorption capacity of biochar produced from different agro-waste towards crystal violet dye.

S. No	Adsorbent	Temperature (^{o}c)	Surface area (m^2/g)	Pore Volume (cm^3/g)	Maximum adsorption capacity (mg/g)	Reference
1.	Sugarcane bagasse biochar	650	–	–	2.94	[90]
2.	Gliricidia sepium (Wood) biochar	700	808	0.890	9.24	[91]
3.	Sugarcane Filter mud biochar	400	19.80	0.087	25.51	[92]
4.	Date palm petioles biochar	700	640	0.403	24.36	[93]
5.	Chinar leaf (Platanus orientalis) biochar	–	–	–	30.1	[94]
6.	Palm Kernel Shell	350	16.04	0.02	24.45	[95]
7.	Coconut Husk Biochar -CHB	340	25.24	0.023	25.15	This study
8.	Lemon wood biochar (Fe_3O_4 modified - magnetic)	700	38.69	0.111	35.31	[96]
9.	Iron oxide impregnated acid treated cornstalk biochar	400	–	–	99.38	[97]
10.	Magnetic nano iron oxide biochar composite - MBC	340	1162.3	0.082	3.63	This study

The consequent narrowing of the pores may render a portion of the previously accessible inner surface area unreachable for CV, leading to a decrease in adsorption capacity. Furthermore, the surface of MBC being negatively charged in aqueous medium may experience electrostatic repulsion to crystal violet, thus lowering its adsorption capacity. Data from adsorption isotherms suggest that unlike CHB, where adsorption of CV involves multiple layers, a monolayer is formed on the surface MBC, consequently adsorption capacity may be further reduced. A reduction of adsorption capacity of biochar on impregnation with iron oxide has been previously reported by Huang et al. [105].

5. Conclusion

This study converted widely available locally sourced agro waste-coconut husk into biochar (CHB). CHB was irregular in shape with uneven edges and a rough and porous surface. Adsorption of CV on to CHB followed Freundlich isotherm model with pseudo second order kinetics and an adsorption maximum of 25.15 mg/g. The process was very rapid initially though a decrease was observed over time probably due to aggregation and the overall process was unfavourable. Moreover, separation of CHB from water was difficult. Thus, unmodified CHB was not suitable for use as an adsorbent for CV. The surface of CHB was modified by deposition of nano iron oxide (Fe_3O_4) on the biochar thus synthesizing MBC. Impregnation with iron oxide increased the bulk density, lowers the pH and average pore diameter of biochar but increases its specific surface area and pore volume. MBC was effective in adsorbing more than 90 % of CV from aqueous solution and followed Langmuir isotherm model with pseudo second order kinetics. It was superparamagnetic and strongly attached to a simple bar magnet which facilitated easy removal from aqueous solution after dye adsorption. This was the first study that demonstrated conversion of coconut husk, an agro-waste, to a magnetic biochar capable of efficiently removing crystal violet from wastewater. However, the magnetization process resulted in a reduction in adsorption capacity. Further research is

Table 4
Comparison of Correlation Coefficients and parameters of different isotherms of CHB and MBC.

	Isotherm	R^2	Parameter	Value
CHB	Freundlich	0.89405	n	0.626
			K_f	2.158
	Langmuir	0.86068	R_l	0.396
			K_l	0.014
	Harkins Jura	0.8577	A	657.9
			B	1.322
	Temkin	0.68574	K_T	0.184
			B_T	241.800
	Elovich	0.7743	Q_{max}	401.6
			K_E	0.0025
	Dubinin Raduskevic	0.46862	K_{DR}	0.0000073
			Q_s	5.426
			E	0.304
MBC	Freundlich	0.91745	n	0.95429
			K_f	1.353
	Langmuir	0.95673	R_l	0.000029
			K_l	689.569
	Harkins Jura	0.80965	A	12.56439
			B	1.46676
	Temkin	0.69385	A_T	0.15891
			B_T	11.81549
	Elovich	0.29393	Q_{max}	75.41478
			K_E	0.0065349
	Dubinin Raduskevic	0.56698	K_{DR}	0.0000109381
			Q_s	2.63517
			E	0.4355927

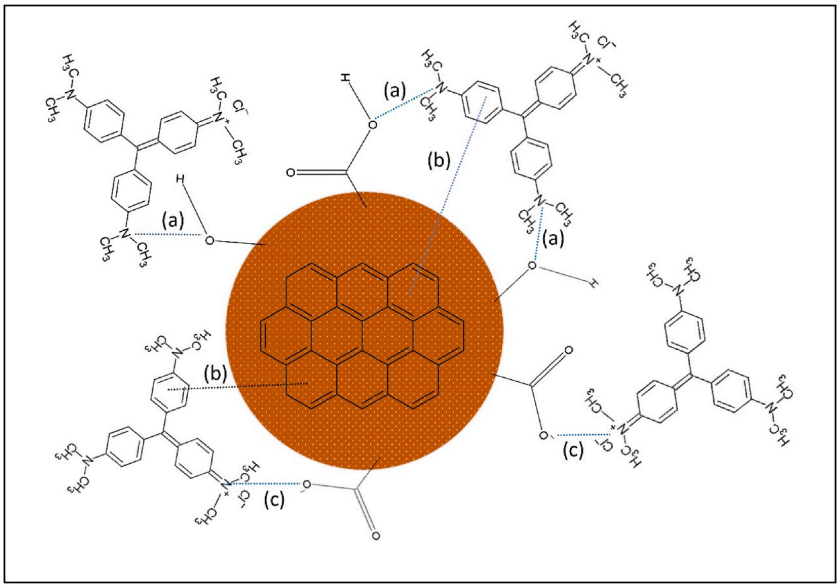

Fig. 10. Possible mechanisms for crystal violet adsorption over coconut husk biochar with (a) hydrogen bonding; (b) π-π interaction and (c) electrostatic attraction. (For interpretation of the references to colour in this figure legend, the reader is referred to the Web version of this article.)

required to optimize the modification of MBC enhance its adsorption capacity without compromising its magnetic properties.

CRediT authorship contribution statement

T. Geetha: Writing – original draft, Visualization, Supervision, Methodology, Data curation, Conceptualization. **John K. Smitha:** Writing – review & editing, Methodology, Conceptualization. **Manju Sebastian:** Writing – review & editing, Data curation. **Mathew Irimpan Litty:** Writing – review & editing, Methodology, Data curation. **Bincy Joseph:** Writing – review & editing. **Jincy Joseph:** Investigation. **T.S. Nisha:** Investigation.

Ethical approval

Not required.

Ethics statement

Not applicable.

Data availability statement

All data analysed in this study are included in the article/supp. material/referenced in article.

Declaration of competing interest

The authors declare that they have no known competing financial interests or personal relationships that could have appeared to influence the work reported in this paper.

Acknowledgment

The authors wish to acknowledge DST- FIST, Department of Science and Technology, Govt. of India [Grant No. SR/FST/College-046/2011] for instrumental facilities, CURIE PG project, Department of Science and Technology, Govt. of India, DBT-STAR College Scheme, Department of Biotechnology, Govt. of India [No. 102/IFD/SAN/3988/201-20 dated February 29, 2020] for supporting the science departments of Vimala College (Autonomous), Thrissur, Kerala, India. Central Sophisticated Instrumentation Facility (CSIF), University of Calicut for SEM and FTIR Data, St. Thomas College (Autonomous), Thrissur for XRD data and Sophisticated Analytical Instrument Facility, IIT Madras for VSM data.

References

[1] M. Roy, F. Shamim, Research on the impact of industrial pollution on river Ganga: a review, International Journal of Prevention and Control of Industrial Pollution 6 (1) (2020) 43–51.
[2] S. Mishra, A. Kumar, Estimation of physicochemical characteristics and associated metal contamination risk in the Narmada River, India, Environmental Engineering Research 26 (1) (2021).
[3] Shahid M. Natasha, S. Khalid, et al., A critical analysis of wastewater use in agriculture and associated health risks in Pakistan, Environ. Geochem. Health 45 (2023) 5599–5618, https://doi.org/10.1007/s10653-020-00702-3.
[4] MdK. Hasan, A. Shahriar, K.U. Jim, Water pollution in Bangladesh and its impact on public health, Heliyon 5 (2019) e02145, https://doi.org/10.1016/j.heliyon.2019.e02145.
[5] M.S.I. Afrad, M.B. Monir, M.E. Haque, et al., Impact of industrial effluent on water, soil and Rice production in Bangladesh: a case of Turag River Bank, J Environ Health Sci Eng 18 (2020) 825–834, https://doi.org/10.1007/s40201-020-00506-8.
[6] H. Zhang, H. Li, H. Yu, S. Cheng, Water quality assessment and pollution source apportionment using multi-statistic and APCS-MLR modeling techniques in Min River Basin, China, Environ. Sci. Pollut. Control Ser. 27 (2020) 41987–42000, https://doi.org/10.1007/s11356-020-10219-y.
[7] R. Jamee, R. Siddique, Biodegradation of synthetic dyes of textile effluent by microorganisms: an environmentally and economically sustainable approach, Eur J Microbiol Immunol (Bp) 9 (2019) 114–118, https://doi.org/10.1556/1886.2019.00018.
[8] A.P. Periyasamy, J. Militky, Sustainability in Textile Dyeing: Recent Developments, 2020, pp. 37–79.
[9] N. Muhd Julkapli, S. Bagheri, S. Bee Abd Hamid, Recent advances in heterogeneous photocatalytic decolorization of synthetic dyes, Sci. World J. 2014 (2014) 1–25, https://doi.org/10.1155/2014/692307.
[10] G. Samchetshabam, Ajmal Hussan, T.G. Choudhury, Impact of textile dyes waste on aquatic environments and its treatment, Environ. Ecol. 35 (3C) (2017) 2349–2353. Environment & Ecology 35:2349-2353.
[11] M. Ismail, K. Akhtar, M.I. Khan, et al., Pollution, toxicity and carcinogenicity of organic dyes and their catalytic bio-remediation, Curr Pharm Des 25 (2019) 3645–3663, https://doi.org/10.2174/1381612825666191021142026.
[12] Y. Miyah, A. Lahrichi, M. Idrissi, et al., Assessment of adsorption kinetics for removal potential of Crystal Violet dye from aqueous solutions using Moroccan pyrophyllite, Journal of the Association of Arab Universities for Basic and Applied Sciences 23 (2017) 20–28, https://doi.org/10.1016/j.jaubas.2016.06.001.
[13] M.T. Amin, A.A. Alazba, M. Shafiq, Successful application of Eucalyptus camdulensis biochar in the batch adsorption of crystal violet and methylene blue dyes from aqueous solution, Sustainability 13 (2021) 3600, https://doi.org/10.3390/su13073600.
[14] A.El Naeem G. Alaa salah omer, A.I. Abd-Elhamid, et al., Adsorption of crystal violet and methylene blue dyes using a cellulose-based adsorbent from sugercane bagasse: characterization, kinetic and isotherm studies, J. Mater. Res. Technol. 19 (2022) 3241–3254, https://doi.org/10.1016/j.jmrt.2022.06.045.
[15] S. Li, Removal of crystal violet from aqueous solution by sorption into semi-interpenetrated networks hydrogels constituted of poly(acrylic acid-acrylamide-methacrylate) and amylose, Bioresour. Technol. 101 (2010) 2197–2202, https://doi.org/10.1016/j.biortech.2009.11.044.
[16] M.R. Kulkarni, T. Revanth, A. Acharya, P. Bhat, Removal of Crystal Violet dye from aqueous solution using water hyacinth: equilibrium, kinetics and thermodynamics study, Resource-Efficient Technologies 3 (2017) 71–77, https://doi.org/10.1016/j.reffit.2017.01.009.
[17] P.S. David, A. Karunanithi, N.N. Fathima, Improved filtration for dye removal using keratin–polyamide blend nanofibrous membranes, Environ. Sci. Pollut. Control Ser. 27 (2020) 45629–45638, https://doi.org/10.1007/s11356-020-10491-y.
[18] E. Oyarce, K. Roa, A. Boulett, et al., Removal of dyes by polymer-enhanced ultrafiltration: an overview, Polymers 13 (2021) 3450, https://doi.org/10.3390/polym13193450.
[19] R. Gusain, K. Gupta, P. Joshi, O.P. Khatri, Adsorptive removal and photocatalytic degradation of organic pollutants using metal oxides and their composites: a comprehensive review, Adv. Colloid Interface Sci. 272 (2019) 102009, https://doi.org/10.1016/j.cis.2019.102009.
[20] O.M. Rodríguez-Narváez, A.R. Picos, N. Bravo-Yumi, et al., Electrochemical oxidation technology to treat textile wastewaters, Curr. Opin. Electrochem. 29 (2021) 100806, https://doi.org/10.1016/j.coelec.2021.100806.
[21] J. Wang, H. Chen, Catalytic ozonation for water and wastewater treatment: recent advances and perspective, Sci. Total Environ. 704 (2020) 135249, https://doi.org/10.1016/j.scitotenv.2019.135249.
[22] S.C.M. Signorelli, J.M. Costa, AF de Almeida Neto, Electrocoagulation-flotation for orange II dye removal: kinetics, costs, and process variables effects, J. Environ. Chem. Eng. 9 (2021) 106157, https://doi.org/10.1016/j.jece.2021.106157.

[23] S.S. Beulah, K. Muthukumaran, Methodologies of removal of dyes from wastewater: a review, Int. Res. J. Pure Appl. Chem. (2020) 68–78, https://doi.org/10.9734/irjpac/2020/v21i1130225.

[24] H. Patel, V.K. Yadav, K.K. Yadav, et al., A recent and systemic approach towards microbial biodegradation of dyes from textile industries, Water (Basel) 14 (2022) 3163, https://doi.org/10.3390/w14193163.

[25] P.S. Kumar, G.J. Joshiba, C.C. Femina, P. Varshini, S. Priyadharshini, M.A. Karthick, R. Jothirani, A critical review on recent developments in the low-cost adsorption of dyes from wastewater, Desalination Water Treat. 172 (2019) 395–416.

[26] N. Tara, S.I. Siddiqui, G. Rathi, et al., Nano-engineered adsorbent for the removal of dyes from water: a review, Curr. Anal. Chem. 16 (2020) 14–40, https://doi.org/10.2174/1573411015666190117124344.

[27] P. Srivatsav, B.S. Bhargav, V. Shanmugasundaram, et al., Biochar as an eco-friendly and economical adsorbent for the removal of colorants (dyes) from aqueous environment: a review, Water (Basel) 12 (2020) 3561, https://doi.org/10.3390/w12123561.

[28] S. Dutta, B. Gupta, S.K. Srivastava, A.K. Gupta, Recent advances on the removal of dyes from wastewater using various adsorbents: a critical review, Mater Adv 2 (2021) 4497–4531, https://doi.org/10.1039/D1MA00354B.

[29] S.H. Alrefaee, M. Aljohani, K. Alkhamis, F. Shaaban, M.G. El-Desouky, A.A. El-Bindary, M.A. El-Bindary, Adsorption and effective removal of organophosphorus pesticides from aqueous solution via novel metal-organic framework: adsorption isotherms, kinetics, and optimization via Box-Behnken design, J. Mol. Liq. 384 (2023) 122206, https://doi.org/10.1016/j.molliq.2023.122206.

[30] A.M. Alsuhaibani, A.A. Alayyafi, L.A. Albedair, M.G. El-Desouky, A.A. El-Bindary, Synthesis and characterization of metal–organic frameworks based on thorium for the effective removal of 2, 4-dichlorophenylacetic pesticide from water: batch adsorption and Box-Behnken Design optimization, and evaluation of reusability, J. Mol. Liq. 398 (2024) 124252, https://doi.org/10.1016/j.molliq.2024.124252.

[31] R. Chikri, N. Elhadiri, M. Benchanaa, Y. El maguana, Efficiency of sawdust as low-cost adsorbent for dyes removal, J. Chem. 2020 (2020) 1–17, https://doi.org/10.1155/2020/8813420.

[32] A. Almahri, K.S. Abou-Melha, H.A. Katouah, A.M. Al-bonayan, F.A. Saad, M.G. El-Desouky, A.A. El-Bindary, Adsorption and removal of the harmful pesticide 2, 4-dichlorophenylacetic acid from an aqueous environment via coffee waste biochar: synthesis, characterization, adsorption study and optimization via Box-Behnken design, J. Mol. Struct. 1293 (2023) 136238, https://doi.org/10.1016/j.molstruc.2023.136238.

[33] P. Adwani, J. Singh, Production of biochar from different feedstocks using various methods and its application for the reduction of environmental contaminants: a review, J. Appl. Sci. Innov. Technol. 2 (1) (2023) 18–24.

[34] P. Rethinam, V. Krishnakumar, Global scenario of coconut and coconut water, in: Coconut Water, Springer International Publishing, Cham, 2022, pp. 17–35.

[35] K.B. Hebbar, P.S. Abhin, Jose V. Sanjo, et al., Predicting the potential suitable climate for coconut (cocos nucifera L.) cultivation in India under climate change scenarios using the MaxEnt model, Plants 11 (2022) 731, https://doi.org/10.3390/plants11060731.

[36] Y. Leow, V. Sequerah, Y.C. Tan, et al., A tough, biodegradable and water-resistant plastic alternative from coconut husk, Compos. B Eng. 241 (2022) 110031, https://doi.org/10.1016/j.compositesb.2022.110031.

[37] M.A. Adebayo, J.M. Jabar, J.S. Amoko, et al., Coconut husk-raw clay-Fe composite: preparation, characteristics and mechanisms of Congo red adsorption, Sci. Rep. 12 (2022) 14370, https://doi.org/10.1038/s41598-022-18763-y.

[38] N. Sahu, S. Shukla, Adsorptive removal of Arsenic (III) from magnetic biochar fabricated from agricultural waste biomass, J. Appl. Sci. Innov. Technol 1 (2) (2022) 52–55.

[39] Stelte Wnrsb, Arsanadi, Coir from coconut processing waste as a raw material for applications beyond traditional uses, Bioresources 18 (2023) 1.

[40] Z. Ren, F. Chen, B. Wang, et al., Magnetic biochar from alkali-activated rice straw for removal of rhodamine B from aqueous solution, Environmental Engineering Research 25 (2019) 536–544, https://doi.org/10.4491/eer.2019.232.

[41] Y. Yi, Z. Huang, B. Lu, et al., Magnetic biochar for environmental remediation: a review, Bioresour. Technol. 298 (2020) 122468, https://doi.org/10.1016/j.biortech.2019.122468.

[42] X. Li, C. Wang, J. Zhang, et al., Preparation and application of magnetic biochar in water treatment: a critical review, Sci. Total Environ. 711 (2020) 134847, https://doi.org/10.1016/j.scitotenv.2019.134847.

[43] B. Xiao, J. Jia, W. Wang, et al., A review on magnetic biochar for the removal of heavy metals from contaminated soils: preparation, application, and microbial response, Journal of Hazardous Materials Advances 10 (2023) 100254, https://doi.org/10.1016/j.hazadv.2023.100254.

[44] J.O. Ighalo, J. Conradie, C.R. Ohoro, J.F. Amaku, K.O. Oyedotun, N.W. Maxakato, K.G. Akpomie, E.S. Okeke, C. Olisah, A. Malloum, K.A. Adegoke, Biochar from coconut residues: an overview of production, properties, and applications, Ind. Crop. Prod. 204 (2023) 117300.

[45] Z. Hao, C. Wang, Z. Yan, H. Jiang, H. Xu, Magnetic particles modification of coconut shell-derived activated carbon and biochar for effective removal of phenol from water, Chemosphere 211 (2018) 962–969.

[46] B.S. Peixoto, L.S. de Oliveira Mota, I.M. Dias, B. Muzzi, M. Albino, M. Petrecca, C. Innocenti, P.C.O. de Oliveira, G.A. Romeiro, C. Sangregorio, M.C. de Moraes, An alternative synthesis of magnetic biochar from green coconut husks and its application for simultaneous and individual removal of caffeine and salicylic acid from aqueous solution, J. Environ. Chem. Eng. 11 (5) (2023) 110835.

[47] Y. Xu, Y. Qu, Y. Yang, B. Qu, R. Shan, H. Yuan, Y. Sun, Study on efficient adsorption mechanism of Pb2+ by magnetic coconut biochar, Int. J. Mol. Sci. 23 (22) (2022) 14053.

[48] A. Punnose, S. Anitha, Production and characterisation of biochar from different organic materials, J. Trop. Agric. 53 (2016) 191–196.

[49] Lagergren Skung, About the theory of so-called adsorption of soluble substances, Sven Vetenskapsakad Handingarl 24 (1898) 1–39.

[50] G. Blanchard, M. Maunaye, G. Martin, Removal of heavy metals from waters by means of natural zeolites, Water Res. 18 (1984) 1501–1507, https://doi.org/10.1016/0043-1354(84)90124-6.

[51] Y.-S. Ho, Second-order kinetic model for the sorption of cadmium onto tree fern: a comparison of linear and non-linear methods, Water Res. 40 (2006) 119–125, https://doi.org/10.1016/j.watres.2005.10.040.

[52] Nguyen X. Cuong, Huyen Nguyen T. Thanh, Chuong Nguyen T. Hong, et al., Sustainable carbonaceous biochar adsorbents derived from agro-wastes and invasive plants for cation dye adsorption from water, Chemosphere 282 (2021) 131009, https://doi.org/10.1016/j.chemosphere.2021.131009.

[53] Y. Yang, X. Lin, B. Wei, et al., Evaluation of adsorption potential of bamboo biochar for metal-complex dye: equilibrium, kinetics and artificial neural network modeling, Int. J. Environ. Sci. Technol. 11 (2014) 1093–1100, https://doi.org/10.1007/s13762-013-0306-0.

[54] H. Freundlich, Adsorption in solution, Phys In Chem Soc 40 (1906) 1361–1368.

[55] I. Langmuir, The adsorption of gases on plane surfaces of glass, mica and platinum, J. Am. Chem. Soc. 40 (1918) 1361–1403, https://doi.org/10.1021/ja02242a004.

[56] K.Y. Foo, B.H. Hameed, Insights into the modeling of adsorption isotherm systems, Chem. Eng. J. 156 (2010) 2–10, https://doi.org/10.1016/j.cej.2009.09.013.

[57] F. Tümsek, Ö. Avcı, Investigation of kinetics and isotherm models for the acid orange 95 adsorption from aqueous solution onto natural minerals, J. Chem. Eng. Data 58 (2013) 551–559, https://doi.org/10.1021/je301215s.

[58] S. Kalam, S.A. Abu-Khamsin, M.S. Kamal, S. Patil, Surfactant adsorption isotherms: a review, ACS Omega 6 (2021) 32342–32348, https://doi.org/10.1021/acsomega.1c04661.

[59] S. Idris, M.M. Ndamitso, Y.A. Iyaka, E.B. Mohammed, Sawdust as an Adsorbent for the Removal of Methylene Blue from Aqueous Solution: Adsorption and Equilibrium Studies, 2012.

[60] S. Rawat, J. Singh, Fabrication of iron nanoparticles by reusing an iron waste and their application as efficient adsorbents to remove crystal violet dye from water, J. Appl. Sci. Innov. Technol 1 (2) (2022) 37–46.

[61] B.S. Trinh, P.T. Le, D. Werner, N.H. Phuong, T.L. Luu, Rice husk biochars modified with magnetized iron oxides and nano zero valent iron for decolorization of dyeing wastewater, Processes 7 (10) (2019) 660.

[62] S. Nirmaladevi, N. Palanisamy, A comparative study of the removal of cationic and anionic dye from aqueous solutions using biochar as an adsorbent, Desalination Water Treat. 175 (2020) 282–292, https://doi.org/10.5004/dwt.2020.24906.

[63] S. Wang, H. Zhao, J. Liu, et al., A study on and adsorption mechanism of ammonium nitrogen by modified corn straw biochar, R. Soc. Open Sci. 10 (2023), https://doi.org/10.1098/rsos.221535.

[64] Z.Z. Chowdhury, M.Z. Karim, M.A. Ashraf, K. Khalid, Influence of carbonization temperature on physicochemical properties of biochar derived from slow pyrolysis of durian wood (Durio zibethinus) sawdust, Bioresources 11 (2016) 3356–3372.

[65] X. Zhang, L. Zhang, A. Li, Eucalyptus sawdust derived biochar generated by combining the hydrothermal carbonization and low concentration KOH modification for hexavalent chromium removal, J. Environ. Manag. 206 (2018) 989–998, https://doi.org/10.1016/j.jenvman.2017.11.079.

[66] N. Chaukura, E.C. Murimba, W. Gwenzi, Synthesis, characterisation and methyl orange adsorption capacity of ferric oxide–biochar nano-composites derived from pulp and paper sludge, Appl. Water Sci. 7 (2017) 2175–2186, https://doi.org/10.1007/s13201-016-0392-5.

[67] C. Wang, L. Li, J. Shi, H. Jin, Biochar production by coconut shell gasification in supercritical water and evolution of its porous structure, J. Anal. Appl. Pyrolysis 156 (2021) 105151, https://doi.org/10.1016/j.jaap.2021.105151.

[68] B. Mahanty, S. Mondal, Synthesis of magnetic biochar using agricultural waste for the separation of Cr(VI) from aqueous solution, Arabian J. Sci. Eng. 46 (2021) 10803–10818, https://doi.org/10.1007/s13369-021-05572-0.

[69] M. Thommes, K. Kaneko, A.V. Neimark, et al., Physisorption of gases, with special reference to the evaluation of surface area and pore size distribution (IUPAC Technical Report), Pure Appl. Chem. 87 (2015) 1051–1069, https://doi.org/10.1515/pac-2014-1117.

[70] L. Leng, Q. Xiong, L. Yang, et al., An overview on engineering the surface area and porosity of biochar, Sci. Total Environ. 763 (2021) 144204, https://doi.org/10.1016/j.scitotenv.2020.144204.

[71] J.-H. Yuan, R.-K. Xu, H. Zhang, The forms of alkalis in the biochar produced from crop residues at different temperatures, Bioresour. Technol. 102 (2011) 3488–3497, https://doi.org/10.1016/j.biortech.2010.11.018.

[72] Younis Uzma, Bokhari Tasveer Zahra, Qayyum Muhammad Farooq, et al., Biochemical characterization of cotton stalks biochar suggests its role in soil as amendment and decontamination. Am Eurasian J, Agric Environ Sci 6 (2017) 127–137.

[73] A.A. Salema, M.T. Afzal, L. Bennamoun, Pyrolysis of corn stalk biomass briquettes in a scaled-up microwave technology, Bioresour. Technol. 233 (2017) 353–362, https://doi.org/10.1016/j.biortech.2017.02.113.

[74] Y. Zheng, Y. Wan, J. Chen, et al., MgO modified biochar produced through ball milling: a dual-functional adsorbent for removal of different contaminants, Chemosphere 243 (2020) 125344, https://doi.org/10.1016/j.chemosphere.2019.125344.

[75] Y. Cai, H. Qi, Y. Liu, X. He, Sorption/desorption behavior and mechanism of NH_4^+ by biochar as a nitrogen fertilizer sustained-release material, J. Agric. Food Chem. 64 (2016) 4958–4964, https://doi.org/10.1021/acs.jafc.6b00109.

[76] S.K. Yong, Jesielyna Leyom, Chia Chay Tay, Suhaimi Abdul Talib, Sorption of lead from aqueous system using cocoa pod husk biochar: kinetic and isotherm studies, Int. J. Eng. Technol. 7 (2018) 241–244.

[77] H.-L. Yan, Z.-M. Zong, Z.-K. Li, et al., Sweet sorghum stalk liquefaction in supercritical methanol: effects of operating conditions on product yields and molecular composition of soluble fraction, Fuel Process. Technol. 155 (2017) 42–50, https://doi.org/10.1016/j.fuproc.2016.02.011.

[78] S. Miri, J.A.E. Perez, S.K. Brar, et al., Sustainable production and co-immobilization of cold-active enzymes from Pseudomonas sp. for BTEX biodegradation, Environ. Pollut. 285 (2021) 117678, https://doi.org/10.1016/j.envpol.2021.117678.

[79] S. Li, Y. Gong, Y. Yang, et al., Recyclable CNTs/Fe3O4 magnetic nanocomposites as adsorbents to remove bisphenol A from water and their regeneration, Chem. Eng. J. 260 (2015) 231–239, https://doi.org/10.1016/j.cej.2014.09.032.

[80] S. Liang, S. Shi, H. Zhang, et al., One-pot solvothermal synthesis of magnetic biochar from waste biomass: formation mechanism and efficient adsorption of Cr (VI) in an aqueous solution, Sci. Total Environ. 695 (2019) 133886, https://doi.org/10.1016/j.scitotenv.2019.133886.

[81] S. Saleh, K.B. Kamarudin, W.A.W.A.K. Ghani, L.S. Kheang, Removal of organic contaminant from aqueous solution using magnetic biochar, Procedia Eng. 148 (2016) 228–235, https://doi.org/10.1016/j.proeng.2016.06.590.

[82] A.M. Dehkhoda, N. Ellis, E. Gyenge, Electrosorption on activated biochar: effect of thermo-chemical activation treatment on the electric double layer capacitance, J. Appl. Electrochem. 44 (2014) 141–157, https://doi.org/10.1007/s10800-013-0616-4.

[83] Y. Yan, S. Manickam, E. Lester, et al., Synthesis of graphene oxide and graphene quantum dots from miscanthus via ultrasound-assisted mechano-chemical cracking method, Ultrason. Sonochem. 73 (2021) 105519, https://doi.org/10.1016/j.ultsonch.2021.105519.

[84] T. Liu, Y. Gu, D.Y. Xing, et al., Rapid and high-capacity adsorption of PFOS and PFOA by regenerable ammoniated magnetic particle, Environ. Sci. Pollut. Control Ser. 25 (2018) 13813–13822, https://doi.org/10.1007/s11356-018-1578-1.

[85] S. Taheri, M.M. Heravi, P. Mohammadi, Synthesis of Ag nanoparticles by Celery leaves extract supported on magnetic biochar substrate, as a catalyst for the reduction reactions, Sci. Rep. 12 (2022) 13678, https://doi.org/10.1038/s41598-022-18131-w.

[86] N. Chaukura, E.C. Murimba, W. Gwenzi, Synthesis, characterisation and methyl orange adsorption capacity of ferric oxide–biochar nano-composites derived from pulp and paper sludge, Appl. Water Sci. 7 (2017) 2175–2186, https://doi.org/10.1007/s13201-016-0392-5.

[87] J. Xie, R. Lin, Z. Liang, et al., Effect of cations on the enhanced adsorption of cationic dye in Fe3O4-loaded biochar and mechanism, J. Environ. Chem. Eng. 9 (2021) 105744, https://doi.org/10.1016/j.jece.2021.105744.

[88] L. Anah, N. Astrini, Isotherm adsorption studies of Ni(II) ion removal from aqueous solutions by modified carboxymethyl cellulose hydrogel, IOP Conf. Ser. Earth Environ. Sci. 160 (2018) 012017, https://doi.org/10.1088/1755-1315/160/1/012017.

[89] M.A. Al-Ghouti, D.A. Da'ana, Guidelines for the use and interpretation of adsorption isotherm models: a review, J. Hazard Mater. 393 (2020) 122383, https://doi.org/10.1016/j.jhazmat.2020.122383.

[90] E.R. Mahdi, E.A. Shihab, A.H. Fahmi, Adsorption of crystal violet dye by biochar produced from sugarcane bagasse under different temperatures, Passer Journal of Basic and Applied Sciences 5 (2) (2023) 422–427.

[91] A. Wathukarage, I. Herath, M.C.M. Iqbal, M. Vithanage, Mechanistic understanding of crystal violet dye sorption by woody biochar: implications for wastewater treatment, Environ. Geochem. Health 41 (2019) 1647–1661.

[92] C.A. Bernardino, C.F. Mahler, M.C. Veloso, G.A. Romeiro, Preparation of biochar from sugarcane by-product filter mud by slow pyrolysis and its use like adsorbent, Waste and Biomass Valorization 8 (2017) 2511–2521.

[93] H.O. Chahinez, O. Abdelkader, Y. Leila, H.N. Tran, One-stage preparation of palm petiole-derived biochar: characterization and application for adsorption of crystal violet dye in water, Environ. Technol. Innovat. 19 (2020) 100872.

[94] F. Ahmad Khan, A. Ahad, S.S. Shah, M. Farooqui, Adsorption of crystal violet dye using Platanus orientalis (Chinar tree) leaf powder and its biochar: equilibrium, kinetics and thermodynamics study, Int. J. Environ. Anal. Chem. 103 (16) (2023) 4820–4840.

[95] P.P. Kyi, J.O. Quansah, C.G. Lee, J.K. Moon, S.J. Park, The removal of crystal violet from textile wastewater using palm kernel shell-derived biochar, Appl. Sci. 10 (7) (2020) 2251.

[96] R. Foroutan, S.J. Peighambardoust, S.H. Peighambardoust, M. Pateiro, J.M. Lorenzo, Adsorption of crystal violet dye using activated carbon of lemon wood and activated carbon/Fe3O4 magnetic nanocomposite from aqueous solutions: a kinetic, equilibrium and thermodynamic study, Molecules 26 (8) (2021) 2241.

[97] P. Sun, C. Hui, R. Azim Khan, et al., Efficient removal of crystal violet using Fe3O4-coated biochar: the role of the Fe3O4 nanoparticles and modeling study their adsorption behavior, Sci. Rep. 5 (2015) 12638, https://doi.org/10.1038/srep12638.

[98] D. Huang, C. Liu, C. Zhang, et al., Cr(VI) removal from aqueous solution using biochar modified with Mg/Al-layered double hydroxide intercalated with ethylenediaminetetraacetic acid, Bioresour. Technol. 276 (2019) 127–132, https://doi.org/10.1016/j.biortech.2018.12.114.

[99] T. Islam, C. Peng, I. Ali, et al., Synthesis of rice husk-derived magnetic biochar through liquefaction to adsorb anionic and cationic dyes from aqueous solutions, Arabian J. Sci. Eng. 46 (2021) 233–246, https://doi.org/10.1007/s13369-020-04537-z.

[100] B. Bhaduri, A.K. Dikshit, T. Kim, K.M. Tripathi, Research progress and prospects of spinel ferrite nanostructures for the removal of nitroaromatics from wastewater, ACS Appl. Nano Mater. 5 (2022) 16000–16026, https://doi.org/10.1021/acsanm.2c02684.

[101] M. Zubair, N.D. Mu'azu, N. Jarrah, N.I. Blaisi, H.A. Aziz, M. A. Al-Harthi, Adsorption behavior and mechanism of methylene blue, crystal violet, eriochrome black T, and methyl orange dyes onto biochar-derived date palm fronds waste produced at different pyrolysis conditions, Water, Air, Soil Pollut. 231 (2020) 1–19.
[102] T.G. Ambaye, M. Vaccari, E.D. van Hullebusch, A. Amrane, S. Rtimi, Mechanisms and adsorption capacities of biochar for the removal of organic and inorganic pollutants from industrial wastewater, Int. J. Environ. Sci. Technol. 18 (10) (2021) 3273–3294.
[103] S. Praveen, J. Jegan, T. Bhagavathi Pushpa, R. Gokulan, L. Bulgariu, Biochar for removal of dyes in contaminated water: an overview, Biochar 4 (2022) 10.
[104] J.O. Eniola, B. Sizirici, A. Khaleel, I. Yildiz, Fabrication of engineered biochar-iron oxide from date palm frond for the effective removal of cationic dye from wastewater, J. Water Proc. Eng. 54 (2023) 104046, https://doi.org/10.1016/j.jwpe.2023.104046.
[105] F. Huang, S.M. Zhang, R.R. Wu, L. Zhang, P. Wang, R.B. Xiao, Magnetic biochars have lower adsorption but higher separation effectiveness for Cd2+ from aqueous solution compared to nonmagnetic biochars, Environ. Pollut. 275 (2021) 116485.